Response of Tropical Rainfall to Reduced Evapotranspiration Depends on Continental Extent

MARIANNE PIETSCHNIG,[a] ABIGAIL L. S. SWANN,[b,c] F. HUGO LAMBERT,[a] AND GEOFFREY K. VALLIS[a]

[a] *Department of Mathematics, University of Exeter, Exeter, United Kingdom*
[b] *Department of Biology, University of Washington, Seattle, Washington*
[c] *Department of Atmospheric Sciences, University of Washington, Seattle, Washington*

(Manuscript received 10 March 2021, in final form 16 July 2021)

ABSTRACT: Future projections of precipitation change over tropical land are often enhanced by vegetation responses to CO_2 forcing in Earth system models. Projected decreases in rainfall over the Amazon basin and increases over the Maritime Continent are both stronger when plant physiological changes are modeled than if these changes are neglected, but the reasons for this amplification remain unclear. The responses of vegetation to increasing CO_2 levels are complex and uncertain, including possible decreases in stomatal conductance and increases in leaf area index due to CO_2 fertilization. Our results from an idealized atmospheric general circulation model show that the amplification of rainfall changes occurs even when we use a simplified vegetation parameterization based solely on CO_2-driven decreases in stomatal conductance, indicating that this mechanism plays a key role in complex model projections. Based on simulations with rectangular continents we find that reducing terrestrial evaporation to zero with increasing CO_2 notably leads to enhanced rainfall over a narrow island. Strong heating and ascent over the island trigger moisture advection from the surrounding ocean. In contrast, over larger continents rainfall depends on continental evaporation. Simulations with two rectangular continents representing South America and Africa reveal that the stronger decrease in rainfall over the Amazon basin seen in Earth system models is due to a combination of local and remote effects, which are fundamentally connected to South America's size and its location with respect to Africa. The response of tropical rainfall to changes in evapotranspiration is thus connected to size and configuration of the continents.

KEYWORDS: Atmosphere; Africa; Amazon region; Maritime Continent; Advection; Atmosphere-land interaction; Convergence/divergence; Vegetation-atmosphere interactions; Climate change; Evaporation; Evapotranspiration; Greenhouse gases; Regional effects; Soil moisture; Surface fluxes; Climate models; General circulation models; Idealized models; Land surface model; Parameterization

1. Introduction

Simulations using Earth system models (ESMs) suggest that the plant physiological response to increasing CO_2 results in an amplification of precipitation changes over the Maritime Continent and the Amazon basin (Swann et al. 2016; Chadwick et al. 2017; Skinner et al. 2017; Kooperman et al. 2018). This means that precipitation (P) decreases more strongly over the Amazon basin and increases more strongly over the Maritime Continent when vegetation changes are included compared to modeling experiments in which these changes are neglected (Chadwick et al. 2017; Kooperman et al. 2018). Several recent studies (Chadwick et al. 2017; Kooperman et al. 2018; Langenbrunner et al. 2019; Saint-Lu et al. 2019) have focused on the response of precipitation to CO_2-driven plant physiological changes in isolation from radiative-transfer changes or vice versa [here: ''physiology''-style simulations and ''radiation''-style simulations, such as ''esmFixClim1'' and ''esmFdBk1,'' respectively, in phase 5 of the Coupled Model Intercomparison Project; Taylor et al. (2012)]. However, a mechanistic understanding of the processes that govern the ΔP amplification due to plant physiological changes over the Amazon basin and the Maritime Continent in full ESM simulations (where both vegetation and radiation components of the models respond to CO_2 forcing) is still lacking (Chadwick et al. 2019).

ESMs include parameterizations of several plant physiological responses to increasing CO_2, which have opposing effects on evapotranspiration (E). On the one hand, plants reduce the aperture of their stomata—small pores on their leaves which regulate the exchange of gases and water with the atmosphere—in response to elevated CO_2 concentrations (Sellers et al. 1996; Ainsworth and Long 2005; Swann 2018). This can result in reduced E over land. On the other hand, CO_2 fertilization can increase the leaf area index (Mahowald et al. 2016; Skinner et al. 2018; Kooperman et al. 2018) especially in water-limited regions (Donohue et al. 2013), which could in turn enhance E. While the net response of vegetation to CO_2 forcing is unclear in natural ecosystems, recent modeling studies suggest that the decrease in stomatal conductance dominate over the increases in leaf area in terms of evapotranspiration in ESMs (Swann et al. 2016; Skinner et al. 2017; Swann 2018; Zarakas et al. 2020).

Supplemental information related to this paper is available at the Journals Online website: https://doi.org/10.1175/JCLI-D-21-0195.s1.

M. Pietschnig's current affiliation: Department of Geosciences, University of Oslo, Oslo, Norway.

Corresponding author: M. Pietschnig, marianne.pietschnig@geo.uio.no

DOI: 10.1175/JCLI-D-21-0195.1

Over land, moisture for rainfall is provided by local evapotranspiration and by advection. Hence, changes in evapotranspiration (ΔE) over continents can have a large impact on ΔP, especially in areas where P depends on E from land surfaces (van der Ent et al. 2010). For example, evaporation from the Amazon rain forest represents a crucial moisture source for local precipitation and for rainfall further downwind in the Río de la Plata basin (Spracklen et al. 2012; Martinez and Dominguez 2014). Loss of the Amazon rain forest through deforestation therefore has the potential to lead to decreases in P not only locally but also further downwind.

The relationship between ΔP and ΔE varies from one tropical land region to another. For example, in the physiology-style ESM simulations, P increases over the Maritime Continent and decreases over the Amazon basin, even though E decreases over both regions (Skinner et al. 2017; Kooperman et al. 2018; Saint-Lu et al. 2019). The increase over the Maritime Continent despite the decrease in E in those simulations has been linked to a warming-induced enhancement of ascent over the islands, which draws in moisture from the surrounding ocean (Kooperman et al. 2018; Saint-Lu et al. 2019; Chadwick et al. 2019). The P decrease over the Amazon basin in those simulations has been connected to circulation changes with enhanced ascent over the Andes driving the P decrease over the Amazon basin (Saint-Lu et al. 2019) or reinforcing it (Langenbrunner et al. 2019).

Using the idealized atmospheric general circulation modeling framework "Isca" (Vallis et al. 2018) we design experiments of varying complexity with Earth-like continents and idealized rectangular, flat continents. We include a simplified parameterization of the vegetation response to increasing CO_2 in Isca, namely an increased resistance to evaporation over land (mimicking a decrease in stomatal conductance at high CO_2), in order to gain an understanding of the ΔP amplification due to vegetation changes over continents of various sizes.

In simulations with realistic continents, we find that including our simple representation of stomatal closure leads to stronger P decreases over parts of the Amazon basin and stronger increases over the Maritime Continent, as expected from ESMs. This suggests that decreases in stomatal conductance (which likely dominate evapotranspiration changes, as discussed above) play a key role in tropical ΔP projections from complex models, consistent with e.g., Swann et al. (2016), Chadwick et al. (2017), and Kooperman et al. (2018) for the Amazon basin. In addition, it means that our idealized model is complex enough to capture the amplification of ΔP seen in ESMs in response to plant physiological changes, while simultaneously being simple enough to allow us to design highly idealized experiments in order to investigate the mechanisms governing these rainfall changes.

In our simulations with rectangular continents, we find that P increases under a doubling of CO_2 for the narrowest continent (with a width comparable to the Philippines). The P increase north of the equator is stronger when land surface evaporation completely ceases in the high CO_2 climate than if terrestrial evaporation remains possible. For wider continents, moisture for rainfall must be provided by continental evaporation and thus P strongly decreases when terrestrial E is switched off at high CO_2.

In Pietschnig et al. (2019), we studied rainfall changes without stomatal closure over two idealized rectangular continents representing Africa and America. We found that warming-induced circulation changes over idealized Africa led to P decreases (i.e., "drying") over idealized America south of the equator (in parts of the "idealized Amazon basin"). In contrast, in the absence of idealized Africa, P increased over idealized America. Here, we find that the strength of this remote drying influence of idealized Africa on the idealized Amazon basin is fairly independent of the vegetation response to CO_2 forcing. However, we find that P decreases—instead of increasing—over parts of the idealized Amazon basin in the absence of Africa when stomatal closure is taken into account. This local drying due to stomatal closure leads to an amplification of the P decrease caused by circulation changes over idealized Africa. The local drying over the idealized Amazon basin due to stomatal closure is fundamentally related to South America's size, as we will show.

2. Methods

We use the modeling framework Isca (Vallis et al. 2018) to design idealized atmospheric general circulation models in order to study the impact of plant physiological changes on continental ΔP. Isca is based on the Flexible Modeling System (https://www.gfdl.noaa.gov/fms/) software infrastructure from the Geophysical Fluid Dynamics Laboratory (GFDL). Various options concerning the configuration of the atmosphere, ocean and land are available in Isca. Earth-like configurations range from aquaplanets (Geen et al. 2018, 2019), via idealized continental shapes (Pietschnig et al. 2019; Laguë et al. 2021) to realistic continents with topography (Geen et al. 2018; Thomson and Vallis 2019; Jiménez-Esteve and Domeisen 2019). In its most realistic Earth-like configuration, Isca compares well to observations and reanalyses (Geen et al. 2018; Thomson and Vallis 2019; Jiménez-Esteve and Domeisen 2019).

In this study, we use the Rapid Radiative Transfer Model (RRTM; Mlawer et al. 1997) and the simplified Betts–Miller convection scheme (Frierson 2007). The model is run at 2.8° × 2.8° horizontal resolution with 40 unevenly spaced vertical levels. Model fields with a vertical component are saved on σ levels by default so we interpolate these fields onto pressure levels, albeit the difference between the original and interpolated fields is generally small for simulations without topography.

Clouds are not represented in our model (although a simple cloud scheme by Liu et al. 2021 is currently being integrated into the modeling framework), but the ocean albedo is set to 0.25 and the albedo of land surfaces is set to 0.33 in all simulations to account for the lack of clouds. While this approach helps moderate the total amount of energy in our simulations, it does not account for cloud feedbacks, which would probably lead to a higher climate sensitivity (more warming), albeit the magnitude of cloud feedbacks in Earth system models remains highly uncertain (Boucher et al. 2013; Zelinka et al. 2020). Furthermore, clouds are modified by land surface temperatures and evaporation and in turn alter the energy input to the surface and atmospheric column, hence affecting the atmospheric circulation and precipitation (Laguë and Swann 2016;

TABLE 1. Experimental configurations in order of their appearance: "lowCO_2" = 300 ppmv CO_2 and zonally symmetric SSTs based on AMIP; "highCO_2" = 600 ppmv CO_2 and zonally symmetric SSTs plus uniform 2.52-K ocean warming.

Name	Continents	Control	Perturbed
RealCont 100%cond	Realistic	C_V = 1.0 and lowCO_2	C_V = 1.0 and highCO_2
RealCont 50%cond	Realistic	C_V = 1.0 and lowCO_2	C_V = 0.5 and highCO_2
6°, 8°, 14°, 25°, 100° xx%cond	Rectangles: 0°–X°E, 30°S–30°N	C_V = 1.0 and lowCO_2	C_V = 0; 0.5; 1.0 and highCO_2
AM xx%cond	Rectangle: 0°–40°E, 30°S–30°N	C_V = 1.0 and lowCO_2	C_V = 0; 0.2; 0.5; 0.7; 1.0 and highCO_2
AF xx%cond	Rectangle: 0°–60°E, 30°S–30°N	C_V = 1.0 and lowCO_2	C_V = 0; 0.2; 0.5; 0.7; 1.0 and highCO_2
2Cont xx%cond	AM + AF at 40°lon apart	C_V = 1.0 and lowCO_2	C_V = 0; 0.2; 0.5; 1.0 and highCO_2
"Physiology"	6°,8°, 14°, 25°, AM, AF, 100°	C_V = 1.0 and lowCO_2	C_V = 0.5 and lowCO_2
"Radiation"	6°,8°, 14°, 25°, AM, AF, 100°	C_V = 1.0 and lowCO_2	C_V = 1.0 and highCO_2

Laguë et al. 2019). In our simulations, sea surface temperatures are prescribed (see section 2a) and thus would not be affected by the presence of clouds.

In Isca, evaporation from the ocean surface is parameterized by the bulk formula:

$$E_{\mathrm{OC}} = \rho C_D |\mathbf{V}| (q_S^* - q) \tag{1}$$

(Vallis et al. 2018). Here, ρ is the density of the atmosphere, C_D is the drag coefficient, $|\mathbf{V}|$ is the magnitude of the velocity, and q is the specific humidity. All of these variables are evaluated in the lowest layer of the atmosphere. The saturation specific humidity at surface temperature is given by q_S^*. Over land, the availability of soil moisture as well as the readiness of plants to evaporate water can reduce evaporation rates compared to the ocean (E_{OC}), so land evaporation (E_L) is parameterized as

$$E_L = C_L E_{\mathrm{OC}}. \tag{2}$$

Here, $C_L \leq 1$ represents the "conductivity" of the land surface to moisture. In the simplest case, C_L can be set to a constant value (Voigt et al. 2016), but this approach yields a zonally uniform P response to CO_2 forcing and does not capture the drying over the Amazon basin (Pietschnig et al. 2019). In the traditional "bucket model" (Manabe 1969), the moisture conductivity $C_L = C_{L,\mathrm{bucket}}$ is determined by the amount of moisture in the soil. Soil moisture is replenished by P and reduced by E. When the soil reaches saturation, excess rainfall is treated as runoff. Where the soil moisture (W in meters) exceeds 75% of the field capacity (W_f), the moisture conductivity $C_{L,\mathrm{bucket}} = 1$. Where this is not the case, $C_{L,\mathrm{bucket}} = W/(0.75W_f)$, which means that E becomes increasingly inhibited as soil moisture decreases (Vallis et al. 2018).

In this study, we introduce another limiting factor for land evaporation in Eq. (2) to represent stomatal closure in response to increasing CO_2, namely the vegetation prefactor C_V. The conductivity C_L thus becomes

$$C_L = C_V C_{L,\mathrm{bucket}}, \tag{3}$$

where C_V represents the impact of stomatal closure on moisture conductance by the land. When C_V is set to 1, land surface evaporation is only limited by soil moisture. When the vegetation prefactor is set to $C_V < 1$, stomatal closure is taken into account in addition to the soil moisture limitation.

a. Model simulations

We run Isca using several different continental configurations starting with realistic continents with topography and then turning to idealized continents of various widths. The simulations for this study are summarized in Table 1. Atmospheric CO_2 concentrations are set to 300 ppmv in the "lowCO_2" climate and a zonally uniform sea surface temperature (SST) climatology based on the Atmospheric Model Intercomparison Project (AMIP, Gates 1992) is prescribed. This SST climatology has its temperature maximum north of the equator in the annual mean. Using zonally uniform SSTs allows us to prescribe the same climatology in simulations with realistic and idealized continents (for further justification, see Pietschnig et al. 2019 or Cook et al. 2004). In the "highCO_2" climate, CO_2 concentrations are doubled to 600 ppmv and a uniform ocean warming of 2.52 K is applied. This warming is equal to the tropical-mean (30°S–30°N) SST increase in an experiment with realistic continents and a seasonal cycle in insolation, where the 20-m-deep thermodynamics-only mixed-layer (or "slab") ocean is free to respond to the doubling of CO_2 (Pietschnig et al. 2019).

The impact of plant physiological changes on continental precipitation is examined using a simple parameterization of stomatal closure. In all simulations, the stomatal conductance is set to 100% in the lowCO_2 climate [i.e., using Manabe's (1969) "bucket" hydrology]. In the highCO_2 climate, stomatal conductance is either held the same at 100% or is reduced to 0%, 20%, 50%, or 70% by setting C_V in Eq. (3) to 1.0, 0.0, 0.2, 0.5, and 0.7, respectively. The model is run for 40 years in the lowCO_2 and highCO_2 climates each, and averages for the respective climate state are taken over years 10–40 of the simulation. Changes in P or E due to the doubling of CO_2 and potential changes in stomatal conductance are calculated as the difference between the highCO_2 and lowCO_2 climates (30-yr averages each). We name the experiments in this study based on the stomatal conductance in the highCO_2 climate, i.e., "50%cond" refers to a simulation with C_V = 0.5 in the highCO_2 climate and C_V = 1.0 in the lowCO_2 climate. The precipitation change is then given by

$$\Delta P_{50\%\mathrm{cond}} = P_{50\%\mathrm{cond}}^{\mathrm{high}CO_2} - P_{100\%\mathrm{cond}}^{\mathrm{low}CO_2}, \tag{4}$$

and equivalently for other degrees of stomatal closure in the highCO_2 climate (i.e., 0%cond, 20%cond and so on).

Based on large-scale CO_2 experiments in natural ecosystems, C_V might lie somewhere between 0.5 and 0.8 for an increase in the CO_2 concentration from 300 to 600 ppm, depending on the plant functional type (Ainsworth and Rogers 2007). The exact value will also vary based on the geographical location and environmental stress factors (Ainsworth and Long 2005; Ainsworth and Rogers 2007). We focus mostly on the 50%cond case because it produces clearer ΔP changes than the 70%cond case, without leading to an extreme drying almost everywhere as in the 20%cond case (see Fig. 3).

First, we conduct a simulation with realistic continents where stomatal conductance remains at 100% in the highCO_2 climate ("RealCont 100%cond," Table 1). The ΔP from this simulation is compared to a simulation with a 50% reduction in stomatal conductance in the highCO_2 climate ("RealCont 50%cond"). Second, we use idealized rectangular flat continents of various widths, which span the entire tropical band (30°S–30°N, see Fig. 3). The narrowest continent covers two grid cells of 2.8° width in the zonal direction, making the island approximately 6° longitude wide (roughly corresponding to the width of the Philippines). Furthermore, we study continents of about 8°, 14°, 25°, 40° (resembling South America, "AM"), 60° (representing Africa, "AF") and 100° longitude. All of those simulations are run with varying degrees of stomatal closure in the highCO_2 climate and 100% conductance at lowCO_2 (Table 1). Following our recent study (Pietschnig et al. 2019), we also investigate rainfall changes for two neighboring continents ("2Cont"): idealized America (AM) and idealized Africa (AF) at the distance of the Atlantic Ocean (40° longitude) apart, with varying stomatal conductances in the highCO_2 climate.

The change in P due to CO_2 forcing in ESMs is often separated into two components: Changes due to the plant physiological response (physiology-style simulations) and changes due to altered radiative transfer (radiation-style experiments, Sellers et al. 1996; Swann et al. 2016; Skinner et al. 2017; Kooperman et al. 2018; Chadwick et al. 2019). To obtain a similar ΔP-decomposition, we perform an additional set of experiments with 50% stomatal conductance in the lowCO_2 climate for each of the idealized continents (Table 1). The "physiology" component of ΔP is then given by

$$\Delta P_{\text{phys}} = P^{\text{lowCO}_2}_{\text{50\%cond}} - P^{\text{lowCO}_2}_{\text{100\%cond}}. \tag{5}$$

The "radiation" component of ΔP can be calculated from our experiments where stomatal conductance stays at 100% in the highCO_2 climate as

$$\Delta P_{\text{rad}} = P^{\text{highCO}_2}_{\text{100\%cond}} - P^{\text{lowCO}_2}_{\text{100\%cond}}. \tag{6}$$

b. The Budyko framework

We study limits on evapotranspiration over land using the Budyko framework. This framework helps categorize land regions as "moisture limited" or "energy limited" (Budyko 1974; Milly 1994; Zhang et al. 2004; Osborne and Lambert 2018). "Potential evaporation" (E_P) is a measure for the amount of energy available for evaporation (Budyko 1974). It is equal to the evaporation that would occur if the surface were saturated (i.e., over oceans or well-watered soils). In regions where E_P (energy available for evaporation) is less than P (moisture available for evaporation), i.e., $E_P/P < 1$, evapotranspiration is classed as energy limited. Where $E_P/P > 1$, evapotranspiration is termed moisture limited in the Budyko framework.

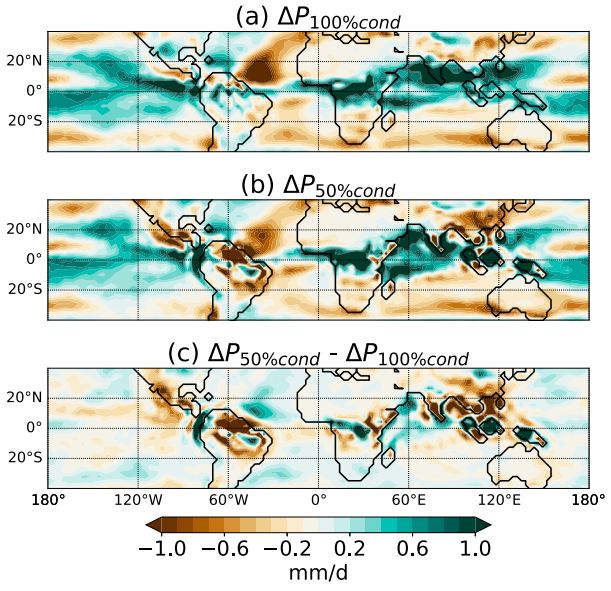

FIG. 1. Annual mean ΔP in response to a doubling of CO_2 for the realistic continents (RealCont) (a) neglecting and (b) including changes in stomatal conductance. In (a) stomatal conductance remains at 100% in the highCO_2 climate ($\Delta P_{100\%\text{cond}}$). In (b) stomatal conductance is reduced to 50% in the highCO_2 climate ($\Delta P_{50\%\text{cond}}$). In both cases, the stomatal conductance is 100% in the lowCO_2 climate and ΔP is calculated using Eq. (4). (c) The difference between the two experiments.

In Isca, we save E_P directly as model output as the evaporation which would occur if the soil were saturated with water [i.e., $C_{L,\text{bucket}} = 1$ in Eq. (3)]. Thus, E_P takes changes in stomatal conductance into account, since $C_L < 1$ when stomatal conductance C_V is reduced even when the bucket is full ($C_{L,\text{bucket}} = 1$). For other Earth system models, E_P is not a standard output and is usually calculated offline (Penman 1948; Monteith 1981; Scheff and Frierson 2014; Milly and Dunne 2016).

3. Results

a. Effect of stomatal closure on precipitation

In our simulation with realistic continents where stomatal conductance is set to 100% throughout the simulation (RealCont 100%cond, Fig. 1a), most equatorial land regions (between 10°S and 10°N) receive more rainfall with warming, except for South America where P decreases to the north and south of the equator. As discussed in detail in Pietschnig et al. (2019), ΔP patterns in this simulation[1] are similar to the CMIP5

[1] "RealCont 100%cond" is simply called "RC" in Pietschnig et al. (2019).

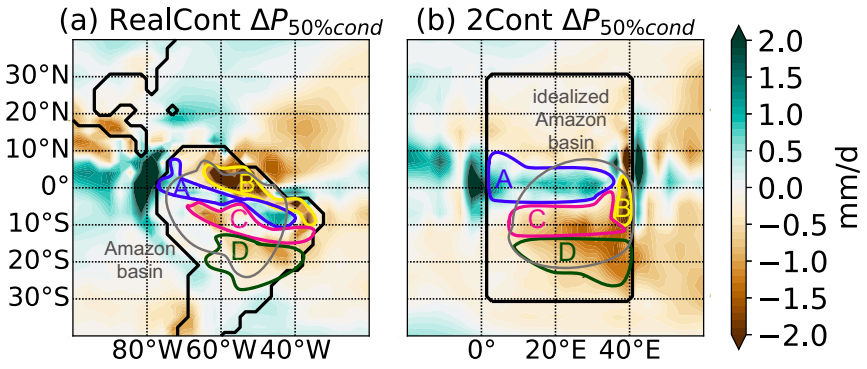

FIG. 2. Annual mean ΔP in response to a doubling of CO_2 including changes in stomatal conductance zoomed in on (a) realistic South America from RealCont (as in Fig. 1b) and (b) idealized America from the simulation with idealized America and Africa (2Cont, as in Fig. 3: 2Cont "50%cond"). The study area is separated into four regions (A, B, C, D) that exhibit similar ΔP features in the realistic and idealized case.

multimodel mean ΔP projections for the RCP8.5 scenario comparing 2081–2100 to 1986–2005 (IPCC 2013).

Here, we focus on the impact of changes in stomatal conductance with increasing CO_2 concentrations on tropical rainfall. We find that taking stomatal closure into account (RealCont 50%cond, Fig. 1b) leads to a much stronger P decrease over equatorial South America than when stomata remain open in the highCO_2 climate (RealCont 100%cond, Fig. 1a). More specifically, stronger drying occurs in the Northeast (area "B" in Fig. 2a), along the southern edge of the Amazon basin and to its East (area "C"), and South of the Amazon basin (area "D"). The area of P increase along the equator in the Amazon basin shifts southeast in 50%cond (area "A") compared to the 100%cond simulation (Fig. 1a). Similar to the amplified drying over large parts of equatorial South America, ΔP is also amplified over the Maritime Continent, with the P increase (i.e., "wetting") being much more pronounced in RealCont 50%cond compared to RealCont 100%cond (Fig. 1). Our simple representation of vegetation in Isca is thus able to capture a sensitivity of ΔP to vegetation changes which is qualitatively similar to complex ESMs. This motivates us to investigate the amplification of ΔP in more idealized simulations in order to understand ESM projections.

In a simulation with two idealized continents representing Africa and South America and 100% stomatal conductance in the highCO_2 climate we find a similar ΔP behavior to the realistic continents. Precipitation P increases over idealized Africa and decreases over parts of idealized America (Fig. 3: row "2Cont,", column "100%cond"). More importantly, when stomatal conductance is reduced to 50% in the highCO_2 climate (Fig. 3: 2Cont, 50%cond), the drying over parts of idealized America is enhanced compared to the 100%cond case, while the African continent shows no clear ΔP response to the change in stomatal conductance. Similar to realistic South America, drying over idealized America is amplified in 2Cont 50%cond in areas C and D (Fig. 2b), and strong drying occurs on the east side of the idealized continent (area B), while P increases along the equator (area A).

Comparable to the realistic Maritime Continent, a very narrow island also sees a P increase with doubling of CO_2 in the 100%cond case, and an even stronger P increase north of the equator when stomatal conductance decreases with warming (Fig. 3: 6°, 50%cond and 100%cond). The strong P increase over the narrow island in the 50%cond case is concentrated north of the equator with drying elsewhere, similar to ΔP over Sumatra in our RealCont 50%cond simulation (Fig. 1), but unlike over Borneo or New Guinea where P increases over the entire island. Differences between the narrow island and realistic Maritime Continent could be caused by the lack of topography, and it would be worth exploring the effect of idealized topography (similar to e.g., Shi and Durran 2014) on ΔP over the narrow continent. Note also that the hemispherically asymmetric ΔP response to increasing CO_2 (strong increases in the Northern Hemisphere tropics over the ocean, which is particularly noticeable in all our idealized simulations) is caused by the prescribed AMIP-derived SST distribution which has its annual mean temperature maximum in the Northern Hemisphere (Pietschnig et al. 2019).

The fact that the idealized continents exhibit a similar ΔP behavior to the realistic continents—which in turn capture some of the behavior of more complex models—suggests that the insight gained from our idealized continent experiments can contribute to our understanding of some of the warming-induced rainfall changes seen in more complex ESMs in response to vegetation changes.

b. *Enhanced precipitation increase over a small island*

Humidity for continental rainfall is provided by moisture advection and by local evapotranspiration. The role of moisture advection for ΔP can be investigated best in the extreme stomatal closure scenario, where no evaporation occurs over land surfaces in the highCO_2 climate (0%cond). Shutting off E over land in the highCO_2 climate results in a P decrease over all land regions for any continent wider than 6° longitude (Fig. 3, column 0%cond). Only the narrowest island sees a strong increase in P north of the equator (Figs. 3 and S1: 6°, 0% cond). It is noteworthy that the P increase in this region is stronger when stomatal conductance is set to zero in the

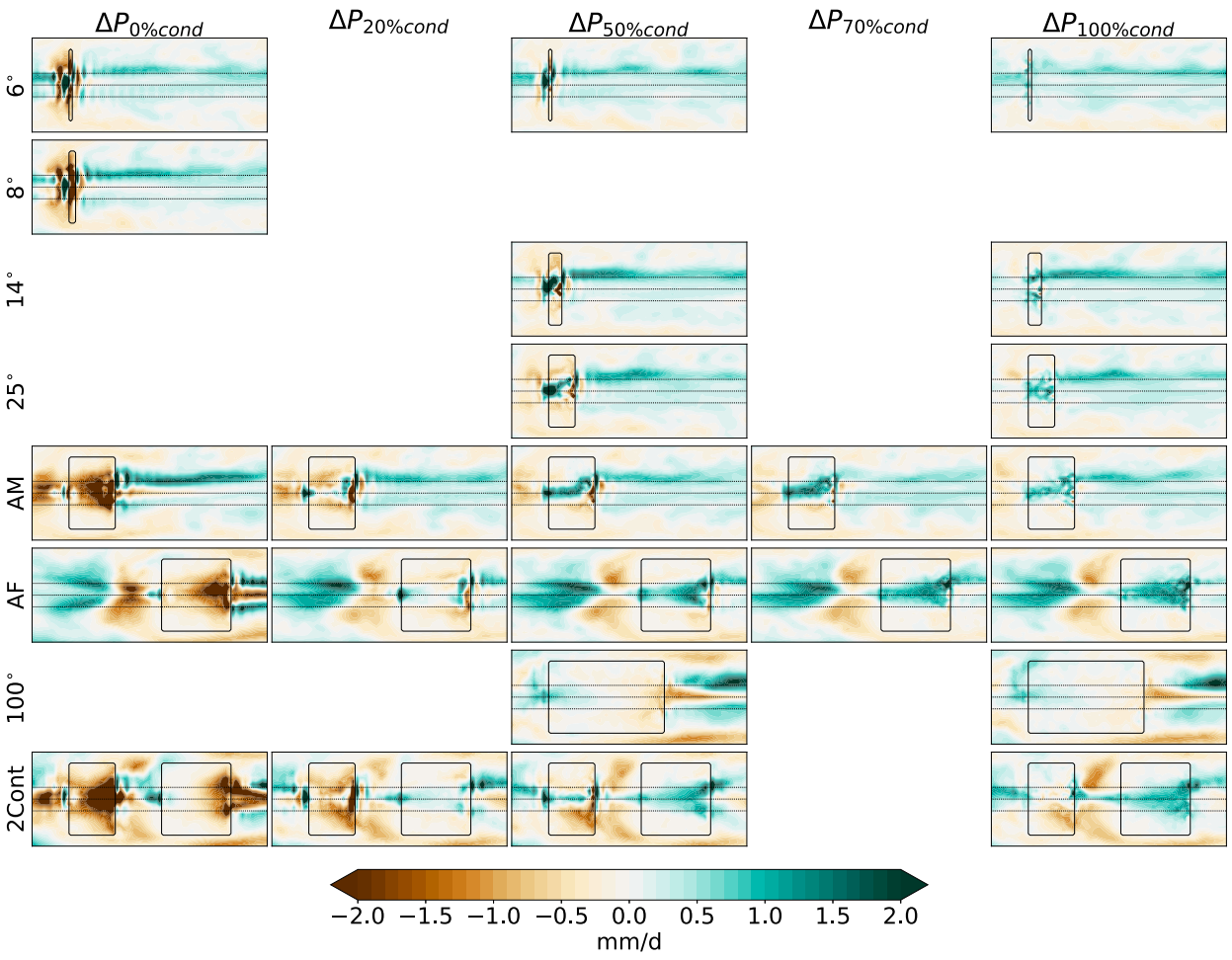

FIG. 3. The ΔP for the idealized continents with different stomatal conductances in the highCO_2 climate (x axis) and different continental widths (y axis). The $\Delta P_{xx\%cond}$ is calculated using Eq. (4) with stomatal conductances of 0%, 20%, 50%, 70%, and 100% (shown from left to right) in the highCO_2 climate, and with 100% stomatal conductance in the lowCO_2 climate in all cases. The three horizontal grid lines are located at 10°S, 0°, and 10°N, and each panel spans 200° in longitude (30°W–170°E).

highCO_2 climate (0%cond) than when the stomata remain open (Fig. S2: 6° and Figs. 3 and S1: row 6°).

For the narrow island (6°) in the 0%cond case, temperatures at the surface and in the lower troposphere increase (Fig. 4a) since the land surface cannot release energy in the form of latent heat through evapotranspiration and instead must release energy as sensible heat (Manabe et al. 1991; Dong et al. 2009). This triggers an enhancement of ascent and low-level convergence over the island, which acts to advect moisture from the surrounding ocean. Relative humidity above about 900 hPa increases (Fig. 5a) and so does P, despite the fact that moisture cannot be provided locally by the land surface. The circulation, moisture convergence and P responses over the 6° continent and the surrounding ocean are stronger when evaporation over land is decreased to zero in the highCO_2 climate than when stomatal conductance remains at 100% (Fig. 4b). Our idealized simulation provides further evidence for the importance of moisture advection for enhanced ΔP over the islands of the Maritime Continent in response to plant physiological changes (Kooperman et al. 2018; Saint-Lu et al. 2019; Chadwick et al. 2019), especially in the extreme case of no terrestrial evapotranspiration.

While the 6° continent gets wetter north of the equator in the experiment with 0% stomatal conductance in the highCO_2 climate, all continents of 8° longitudinal extent or more get drier everywhere (Fig. 3: column 0%cond and Fig. S2). For all continents wider than 6° longitude, moisture advection from the ocean is clearly not sufficient to increase P over land with warming. Instead, local evapotranspiration (which does not occur in the 0%cond experiments) is required to provide moisture for rainfall.

Thus, in terms of ΔP there is a balance between the width of the continent and the degree of stomatal closure with increasing CO_2. A very narrow continent sees a strong P increase when stomatal conductance completely ceases with the CO_2 perturbation (0%cond), whereas wider continents dry out in this experiment. In simulations where stomatal conductance stays at 100% in the highCO_2 climate P is able to increase in the

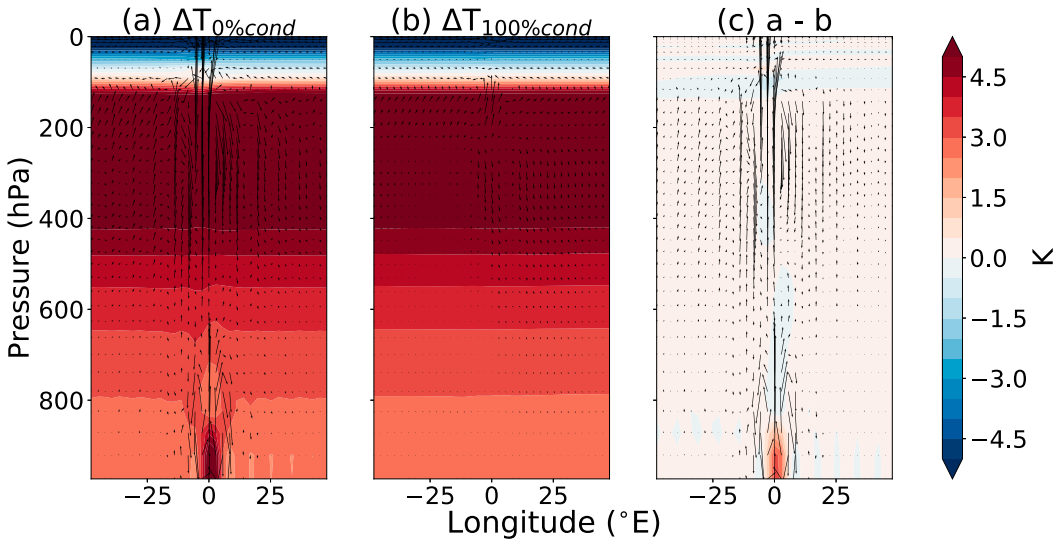

FIG. 4. Doubling of CO_2 induced changes in annual mean temperature (ΔT; colors; K) and the zonal circulation (vectors) averaged over 10°S–10°N for the narrowest continent (6° longitude) with (a) 0% and (b) 100% stomatal conductance in the highCO_2 climate, and (c) the difference between the two cases. The continent is located at 0° longitude. The change in the vertical velocity has been amplified by a factor of 3000 following Nie et al. (2010).

entire equatorial band even over wide continents such as idealized Africa, but the P increase is weaker in some regions than for a moderate (50%cond) or in the case of the narrow island even a full (0%cond) closure of stomata (Fig. 3).

c. *Amplified drying of the Amazon basin*

We now turn to the enhancement of the drying over South America in response to stomatal closure projected by ESMs. As discussed in section 3a, we find that this amplification of ΔP over the Amazon basin is captured in Isca with two idealized continents (2Cont): the drying over parts of the Amazon basin is stronger in 2Cont 50%cond than in 2Cont 100%cond (Fig. 3). This motivates us to focus on setups with one and two of the idealized continents to gain a better understanding of the drying over the Amazon basin.

In Pietschnig et al. (2019), we found that warming-induced enhancement of ascent and rainfall over idealized Africa led to subsidence and a decrease in P over the Atlantic Ocean and over idealized America in areas C and D of Fig. 2b, due to a Matsuno–Gill-type circulation anomaly (Gill 1980). In the absence of idealized Africa, idealized America received more rainfall in the entire equatorial band (Fig. 3: 100%cond,

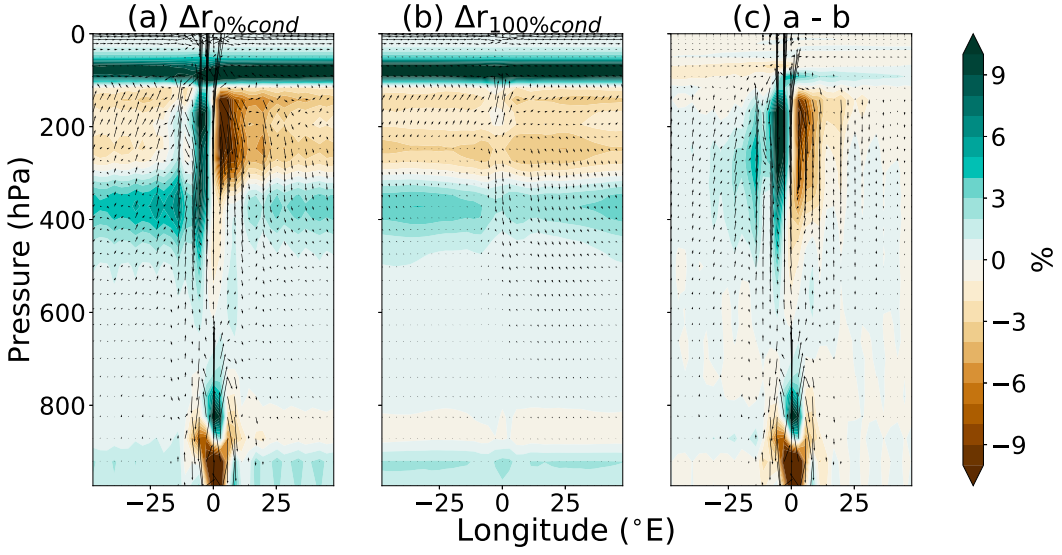

FIG. 5. As in Fig. 4, but with changes in relative humidity (Δr in absolute %) instead of ΔT.

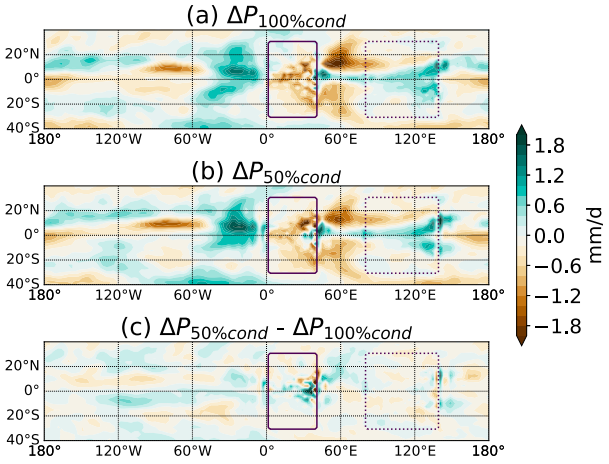

FIG. 6. Impact of idealized Africa on annual mean ΔP over idealized America. The experiment with only America is subtracted from the experiment with both continents [2Cont − AM, see also Pietschnig et al. (2019)] for the case where stomatal conductance (a) remains at 100% in the highCO_2 climate ($\Delta P_{100\%\text{cond}}$) and (b) where it is reduced to 50% [$\Delta P_{50\%\text{cond}}$ from Eq. (4)]. (c) The difference between the 100%cond and 50%cond experiments.

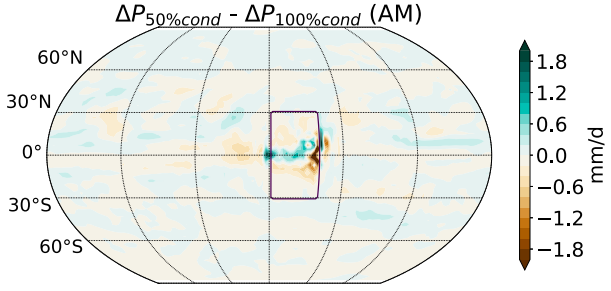

FIG. 7. The difference in precipitation changes over individual idealized America (AM) with a doubling of CO_2 when stomata are partly closed in the highCO_2 climate (50%cond) minus when they remain open (100%cond).

compare AM with 2Cont). The simulations in Pietschnig et al. (2019) are equal to the 100%cond experiments in the present study, since no changes in stomatal conductance occurred.

Interestingly, the strength of the Matsuno–Gill-type teleconnection between idealized Africa and America turns out to be largely independent of stomatal closure: Fig. 6 shows the drying influence of idealized Africa on idealized America for the case where stomata remain open (Fig. 6a) and where stomata are partly closed in the highCO_2 climate (Fig. 6b). The difference between those two simulations (Fig. 6c) is generally small or even positive (i.e., the drying influence is weaker in those areas in the 50%cond case). Hence, the additional decrease in P over parts of the idealized Amazon basin (in areas B, C and D) when stomata are partly closed compared to when they remain open must largely be the result of local changes, rather than changes in the strength of the teleconnection. We therefore investigate P changes over the idealized American continent in isolation (AM).

Over individual idealized America, P increases in the equatorial band under a doubling of CO_2 when stomata remain open (Fig. 3: AM, 100%cond). In contrast, P decreases over parts of the idealized Amazon basin (areas B, C, D) when stomata are partly closed in the highCO_2 climate (Fig. 3: AM, 50%cond). The difference between these two simulations is shown in Fig. 7. Over idealized Africa in the equatorial band, P increases roughly by the same amount with doubling of CO_2 in the 50%cond and 100%cond experiments (Figs. 8 and 3: row AF). The ΔP over idealized America thus exhibits a stronger sensitivity to changes in stomatal conductance than over idealized Africa in the equatorial band.

Changes in ΔE and ΔP tend to be tightly linked over land, since E provides moisture for P, and P provides soil moisture for E. Over idealized Africa in the equatorial band, P and E both increase with the doubling of CO_2 in both the 100%cond and 50%cond cases (Figs. 3 and S3, row AF). Over idealized America along the equator (area A), P and E increase in 100%cond, but P increases much more in the 50%cond experiment compared to 100%cond, despite the weak increase in E in 50%cond. In the case with stomatal closure (50%cond), moisture for precipitation is thus not provided locally by evapotranspiration, but instead by moisture convergence from surrounding areas (Fig. 9). Moisture diverges out of areas B and parts of C and converges toward the equator (area A). The moisture divergence out of areas B and C toward the equator

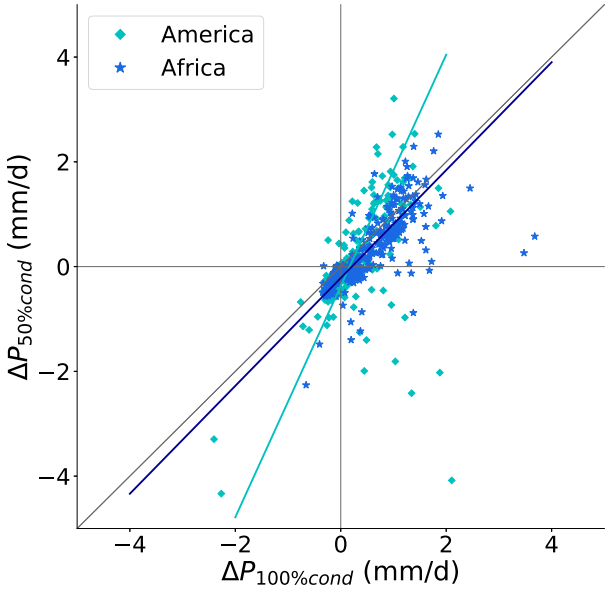

FIG. 8. Annual mean ΔP for all land points between 10°S and 10°N for individual idealized America (cyan diamonds) and idealized Africa (blue stars). The case where stomatal conductance is reduced to 50% in the highCO_2 climate [$\Delta P_{50\%\text{cond}}$ from Eq. (4), y axis] is plotted against the case where stomatal conductance remains at 100% ($\Delta P_{100\%\text{cond}}$, x axis). Total least squares regressions were used to fit the linear regressions. The black line represents $y = x$. The slope of the line for idealized Africa is $k = 1.03$ with a correlation coefficient of $r = 0.77$. For idealized America, the slope of the line is 2.21, and $r = 0.56$.

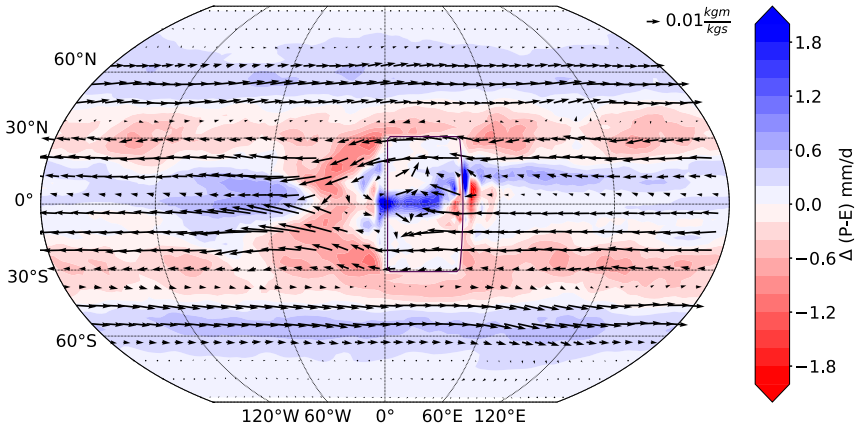

FIG. 9. Colors show changes in the annual mean column-integrated moisture flux convergence or $\Delta(P - E)$ (see e.g., Wills and Schneider 2015), and arrows show changes in the 870-hPa moisture flux $\Delta(q\mathbf{u})$ for idealized America when stomatal closure is reduced to 50% in the highCO_2 climate.

leads to unfavorable conditions for rainfall in those regions in the 50%cond experiment.

But why does E not increase in-step with P over idealized America in 50%cond as it does over idealized Africa? Fundamentally, this can only be related to the different continental extents because this is the only difference between the two. We find that the narrower the continent, the more rainfall it receives in the equatorial band (Fig. 10). The relationship between continental width and rainfall in the equatorial band can be further explained by the fact that the total energy input into the atmospheric column is greater the narrower the continent (Figs. S4 and S5). Stronger low-level convergence and precipitation can therefore be expected to occur in the equatorial region of narrower compared to wider continents [provided that the gross moist stability is small, Neelin and Held (1987) and see the online supplemental material]. Hence, because idealized America is narrower than idealized Africa, it receives more rainfall in the lowCO_2 climate. This finding is important because it helps explain the relatively weak increase in E along the equator over idealized America, as we will now show.

In the Budyko framework, evaporation can be thought of as limited by the available energy at the surface on the one hand, and by available soil moisture on the other (see section 2b). In the lowCO_2 climate, evaporation over idealized Africa can clearly be considered to be moisture limited ($E_P/P > 1$, Fig. 11). Over idealized America along the equator (area A), E is moisture limited in the lowCO_2 climate, but close to the energy-limited regime ($E_P/P < 1$) due to higher P (Fig. 10). A large amount of P leads to a smaller value of E_P/P directly, as the denominator is large. In addition, surface temperatures—and thus E_P—over land tend to be low where P is high, particularly in the equatorial band (Fig. S6).

With the strong increase in P in area A in the 50%cond simulation, this region becomes energy limited in the highCO_2 climate (Figs. 11 and S7). In contrast, over idealized Africa E stays moisture limited in the highCO_2 climate for 50%cond. When E is limited by moisture, E and P increase in step (in the 100%cond case for both idealized America and Africa, Fig. 11), but when E becomes energy limited in AM 50%cond, it cannot keep up with P. Thus, moisture for the strong P increase in area A must be provided by advection from surrounding land areas and from the ocean, instead of by local E. Moisture diverges out of areas B and the eastern part of C, leading to unfavorable conditions for rainfall there (Fig. 9). In addition to those smaller-scale dynamics between area A ($P - E$ increase) and B/C ($P - E$ decrease), the moisture budget decomposition following Seager et al. (2010) (see the online supplemental material) reveals that changes in the circulation contribute to the decrease in $P - E$ in area B/C in the 50%cond case, and the increase in area A (Figs. S8 and S9).

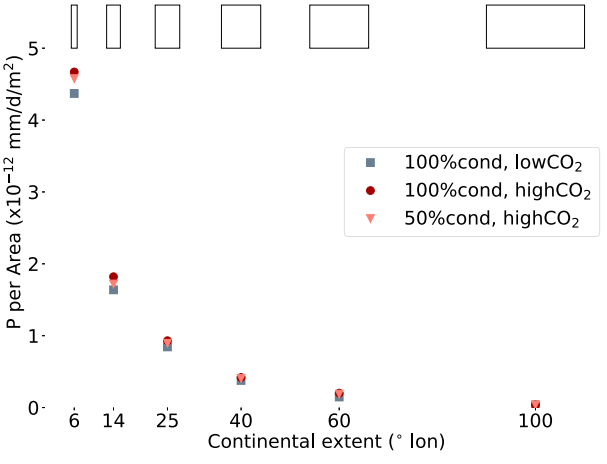

FIG. 10. Annual mean, area weighted average (from 10°S to 10°N) P for different continental extents for the lowCO_2 climate with completely open stomata (100%cond, gray squares) and the highCO_2 climates (100%cond, red circles and 50%cond, salmon triangles). The sizes of the continents are shown at the top of the figure.

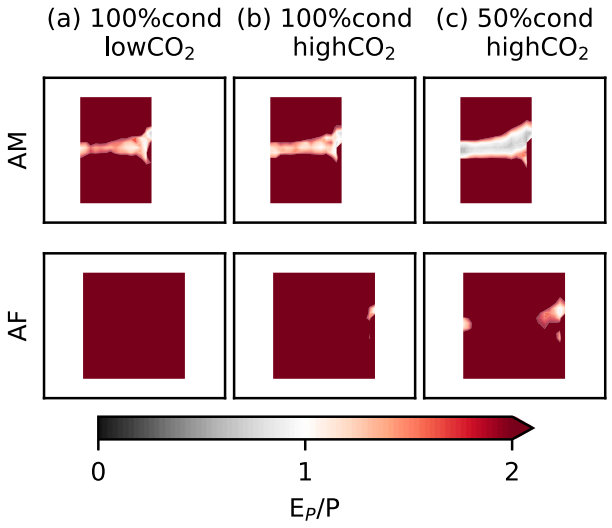

FIG. 11. Moisture (red) and energy (gray) limited regions over idealized America (AM) and idealized Africa (AF) in (a) the lowCO_2 climate with 100% stomatal conductance and the highCO_2 climates with (b) 100% and (c) 50% stomatal conductance. White areas lie between the moisture and energy limit.

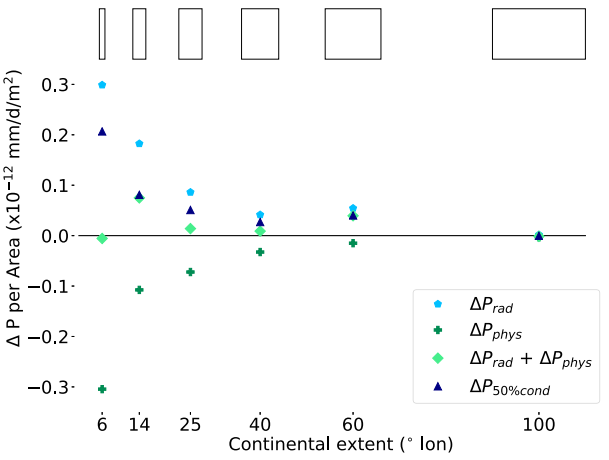

FIG. 12. Decomposition of area-averaged (between 10°S and 10°N) annual mean ΔP for the 50%cond experiment [$\Delta P_{50\%\text{cond}}$ from Eq. (4), dark blue triangles] into the components due to "physiology" [ΔP_{phys} from Eq. (5), dark green crosses] and "radiation" [ΔP_{rad} from Eq. (6), light blue pentagons], and their linear addition ($\Delta P_{\text{rad}} + \Delta P_{\text{phys}}$, light green diamonds). The sizes of the continents are shown at the top of the figure.

It remains an open question for future work to understand why P increases so strongly in area A in the first place in AM 50%cond, and whether there is actually a causal relationship between this increase in P and the enhanced moisture divergence out of areas B/C. It is also possible that the moisture divergence in areas B/C occurs first, leading to stronger moisture convergence into area A. Simulations with higher temporal resolution will provide further insight into the underlying mechanisms.

Returning to the two continents experiment discussed at the start of this section, the stronger P decrease over parts of the idealized Amazon basin (areas B, C, and D) in 2Cont 50%cond compared to 2Cont 100%cond can be understood as a combination of local drying due to stomatal closure (mostly in areas B and C), and a remotely forced drying due to circulation changes over Africa (mostly responsible for the drying in areas C and D). The latter occurs to a similar degree in the 100%cond and 50%cond experiments, as discussed above (Fig. 6). The remotely forced and the local drying combine almost linearly to give the full P response over areas C and D of the idealized Amazon basin (see Fig. S10 in the online supplemental material).

For the realistic continents, changes in moisture flux convergence and limits on evaporation are comparable to our idealized experiments (see Figs. S11 and S12). This suggests that a similar mechanism might contribute to the amplified drying over the Amazon basin in ESMs, although this needs to be investigated further in a separate study using complex simulations.

d. Radiation versus physiology

Intuitively, one might expect a 50% decrease in stomatal conductance to result in a P decrease over all continents, due to restricted evaporation. However, P and E both increase over parts of each individual continent between 10°S and 10°N (Figs. 3 and S3: row 6° to AF, column 50%cond). The radiation and physiology experiments help decompose ΔP into the contributions from changes in radiative transfer (ΔP_{rad}) and stomatal conductance (ΔP_{phys}). Figure 12 shows that stomatal closure on its own leads to a P decrease on average in the equatorial band (albeit some areas receive more P, see Fig. S13), whereas the change in radiative transfer alone leads to a P increase for each individual continent (see also Fig. 3: column 100%cond). For idealized Africa, and for the 14° and 100° continents the two components add linearly to give the full ΔP response (Fig. 12). For the other continents the full response lies somewhere between the physiology and radiation responses. This indicates that the full ΔP is a combination of increasing P due to changes in the radiative transfer, and the stomatal closure induced P decrease, but nonlinear effects are not negligible.

Our radiation and physiology experiments can be compared to their equivalents in Swann et al. (2016), Skinner et al. (2017), Kooperman et al. (2018) and Chadwick et al. (2019), albeit the experiments have slightly different names there. For the radiation experiments, our findings are consistent with these studies over the Maritime Continent and equatorial Africa with increases in all cases (Fig. 12: 6° and 60°, and Fig. 3: 6°, 100%cond and AF, 100%cond). However, for individual idealized America P increases in our radiation simulation (Fig. 12, 40° and Fig. 3: AM, 100%cond) but decreases over the Amazon basin in the equivalent experiments from Swann et al. (2016) and Kooperman et al. (2018). This is likely due to the presence of Africa in the ESMs, which has a drying influence on South America as discussed in previous sections.

The decreases in P in our physiology experiments over large parts of idealized America and Africa are consistent with the equivalent ESM experiments from Swann et al. (2016),

Kooperman et al. (2018) and Chadwick et al. (2019). Over the Maritime Continent, however, the physiology response alone is sufficient to enhance the circulation and rainfall in ESMs, whereas in our idealized simulations with a narrow island radiative transfer changes are required to produce a clear P increase (cf. row 6°, column 50%cond from Fig. S13 and Fig. 3). This discrepancy is possibly due to the lack of topographic features on our idealized continent (similar to the discussion in section 3a), which should be explored in future work. In summary, whether an individual continent sees an increase or a decrease in P in the equatorial band with increasing CO_2 depends on the balance between the drying due to the physiology component, and wetting due to the radiation component.

4. Conclusions

The motivation for this study was to understand the projected amplification of precipitation decreases over the Amazon basin and increases with warming over the Maritime Continent seen in Earth system models in response to plant physiological changes (Swann et al. 2016; Chadwick et al. 2017; Skinner et al. 2017; Kooperman et al. 2018). Using Isca (Vallis et al. 2018), we design idealized atmospheric general circulation models with realistic continents and idealized rectangular continents of varying width. We include a simple parameterization of vegetation that represents changes in stomatal conductance in response to CO_2 forcing.

In a simulation with realistic continents and topography, a 50% reduction in stomatal conductance with a doubling of CO_2 results in stronger and more widespread drying over the Amazon basin and stronger wetting over the Maritime Continent than when the vegetation changes are neglected, in accordance with ESM projections. This provides further evidence that the land surface influences atmospheric processes (Shukla and Mintz 1982; Bonan 2008; Pietschnig et al. 2019; Laguë et al. 2019), and that changes in stomatal conductance play a key role in the projected ΔP amplification. Furthermore, the stronger drying over parts of the Amazon basin in response to a decrease in stomatal conductance implies that deforestation in the Amazon basin could result in strong precipitation decreases (van der Ent et al. 2010; Spracklen et al. 2012; Wright et al. 2017), since evaporation is higher over rain forests compared to tropical pastures in the Amazon basin (von Randow et al. 2004; Bonan 2008).

The simulations with two rectangular, flat continents representing Africa and America, and with a single narrow continent roughly as wide as the Philippines show a similar sensitivity of ΔP to vegetation changes compared to their realistic counterparts. This suggests that our idealized model simulations present valuable tools for understanding the processes dominating precipitation changes in the realistic simulations and in ESMs.

The narrow continent experiences a much stronger P increase north of the equator when stomata are completely closed with warming (and thus no evaporation occurs over land) than when stomata remain open (allowing for moisture to be provided locally). Ascent increases over the continent due to increasing surface temperatures caused by the lack of evaporation over land. The increase in ascent leads to moisture advection onto the island from the surrounding ocean, indicating that local moisture is less important than additional uplift for driving precipitation changes over narrow landmasses in the tropics. This finding confirms recent studies by Kooperman et al. (2018), Chadwick et al. (2019), and Saint-Lu et al. (2019) even for our extreme case of no terrestrial evapotranspiration.

In a simulation with idealized Africa and America and no change in stomatal conductance with warming, a Matsuno–Gill-type circulation anomaly over idealized Africa leads to subsidence and drying over parts of the idealized Amazon basin in areas C and D of Fig. 2b (Pietschnig et al. 2019). The strength of this teleconnection remains largely unchanged when stomatal conductance is reduced by 50% in the highCO_2 climate. The stronger drying over parts of the idealized Amazon basin in the stomatal-closure experiment, particularly in areas B and C, compared to the simulation where stomata remain open must therefore be attributable to local changes.

Over idealized America in isolation, rainfall increases with a doubling of CO_2 when stomata remain open. When stomatal conductance is reduced at high CO_2, rainfall decreases over large parts of the idealized Amazon basin (areas B, C, and D). Along the equator, however (area A), rainfall increases strongly when stomatal conductance is reduced. In this case, evaporation near the equator does not increase in-step with precipitation. Moisture for the increase in rainfall must instead be provided by advection from surrounding land regions (areas B and parts of C), inhibiting rainfall there, or from the ocean. We find that high rainfall rates in the lowCO_2 climate are likely the underlying reason for the weak increase in evaporation along the equator and thus could contribute to the drying of the Amazon basin. The high rainfall rates in the unperturbed climate are a consequence of idealized America's limited longitudinal extent compared to idealized Africa. Thus, the ΔP behavior in response to vegetation changes over the idealized Amazon basin is connected to the continental extent of South America. Furthermore, we find that changes in the circulation also contribute to the increase in $P - E$ in area A, and the $P - E$ decrease in areas B/C.

Changes in P in response to a doubling of CO_2 can be split into two components (Swann et al. 2016; Skinner et al. 2017; Kooperman et al. 2018; Chadwick et al. 2019): the contribution from changes in the radiative transfer (''radiation'') and the contribution from stomatal closure (''physiology''). Our results show that the radiative-transfer changes alone lead to an increase in P, whereas the changes in stomatal conductance alone lead to a general drying over each individual idealized continent. For some of the continents, the full response to a doubling of CO_2 with a 50% decrease in stomatal conductance is a linear combination of those two effects, but nonlinear contributions cannot be neglected in general.

While providing insight into the mechanisms that contribute to the amplification of precipitation change with stomatal closure over the Maritime Continent and the Amazon basin, this study also raises new questions for future research. We hypothesize that the weak increases in evaporation along the equator over idealized America (area A) might lead to moisture divergence out of areas B and C in the idealized Amazon

basin, resulting in drier conditions there. In this study, we have not explicitly shown the chain of causality and it is possible that the moisture divergence in areas B and C occurs first, leading to (rather than lagging) the strong precipitation increase along the equator, or that there is no relationship between the enhanced divergence (areas B/C) and increased precipitation (area A) at all. We further note that circulation changes also contribute to enhanced moisture convergence into area A and divergence from area B (and parts of C). In a separate study we plan to use data with higher temporal resolution, particularly immediately after the climate perturbation occurs, in order to determine which changes occur first and to find causal relationships. In addition, complex Earth system models should be used in future work in order to test whether similar mechanisms are at play in the real-world Amazon basin.

We have also related the net energy input into the atmospheric column to the amount and location of maximum rainfall for the idealized continents, but a more in-depth analysis of the atmospheric energy budget and moisture transports in relation to continental rainfall and precipitation changes will be the subject of our next study. Another interesting avenue for future research would be to explore the effects of idealized topography (similar to e.g., Shi and Durran 2014) on precipitation changes over the Maritime Continent and idealized America. Finally, our simulations did not include any representation of clouds, and studying the impact of cloud feedbacks on precipitation changes in our idealized simulations certainly poses an interesting topic for future research. However, since our results with realistic continents qualitatively agree with complex model projections of tropical precipitation change and due to the high uncertainty connected to cloud feedbacks in Earth system models (Boucher et al. 2013; Zelinka et al. 2020) this study—despite the lack of clouds—provides relevant insight into rainfall changes for different degrees of stomatal closure over continents of various sizes, and contributes to our understanding of tropical precipitation change.

Acknowledgments. This study was partly funded by the University of Exeter College of Engineering, Mathematics and Physical Sciences, by NERC (NE/M009599/1 and NE/N018486/1) and by the U.K.–China Research and Innovation Partnership Fund through the Met Office Climate Science for Service Partnership (CSSP) China as part of the Newton Fund. MP would like to express her gratitude to the Rupert Ford Award, administered by the Royal Meteorological Society and to the University of Exeter College of Engineering, Mathematics and Physical Sciences Ph.D. Mobility Fund for their generous support of her research visit to the University of Washington to work with ALSS. ALSS acknowledges support from National Science Foundation Award AGS-1553715 to the University of Washington. MP would like to acknowledge the use of the University of Exeter High-Performance Computing (HPC) facility in carrying out this work. The authors thank Mike Byrne for his suggestion regarding the moisture budget decomposition and Ruth Geen for sharing parts of her code. Finally, the authors express their gratitude to two anonymous reviewers for their constructive comments on the manuscript. There are no conflicts of interest or competing interests for this work. The manuscript and figures were prepared by MP, data analysis/interpretation was carried out together with ALSS, FHL, and GKV. In addition, ALSS, FHL, and GKV helped design the study and provided feedback on the manuscript drafts. This manuscript is partly based on MP's dissertation (Pietschnig 2020), where further details on the methods can also be found.

Data availability statement. The data for this publication are freely available on Zenodo:
lowCO_2 climate part 1: 10.5281/zenodo.5109451,
lowCO_2 climate part 2: 10.5281/zenodo.5109484,
highCO_2 climate part 1: 10.5281/zenodo.5109489,
highCO_2 climate part 2: 10.5281/zenodo.5109494, and
highCO_2 climate part 3: 10.5281/zenodo.5109502.

REFERENCES

Ainsworth, E. A., and S. P. Long, 2005: What have we learned from 15 years of free-air CO_2 enrichment (FACE)? A meta-analytic review of the responses of photosynthesis, canopy properties and plant production to rising CO_2. *New Phytol.*, **165**, 351–372, https://doi.org/10.1111/j.1469-8137.2004.01224.x.

——, and A. Rogers, 2007: The response of photosynthesis and stomatal conductance to rising [CO_2]: Mechanisms and environmental interactions. *Plant Cell Environ.*, **30**, 258–270, https://doi.org/10.1111/j.1365-3040.2007.01641.x.

Bonan, G. B., 2008: Forests and climate change: Forcings, feedbacks, and the climate benefits of forests. *Science*, **320**, 1444–1449, https://doi.org/10.1126/science.1155121.

Boucher, O., and Coauthors, 2013: Clouds and aerosols. *Climate Change 2013: The Physical Science Basis*, T. F. Stocker et al., Eds., Cambridge University Press, 571–657.

Budyko, M. I., 1974: *Climate and Life*. Academic Press, 507 pp.

Chadwick, R., H. Douville, and C. B. Skinner, 2017: Timeslice experiments for understanding regional climate projections: Applications to the tropical hydrological cycle and European winter circulation. *Climate Dyn.*, **49**, 3011–3029, https://doi.org/10.1007/s00382-016-3488-6.

——, D. Ackerley, T. Ogura, and D. Dommenget, 2019: Separating the influences of land warming, the direct CO_2 effect, the plant physiological effect, and SST warming on regional precipitation changes. *J. Geophys. Res. Atmos.*, **124**, 624–640, https://doi.org/10.1029/2018JD029423.

Cook, K. H., J.-S. Hsieh, and S. M. Hagos, 2004: The Africa–South America intercontinental teleconnection. *J. Climate*, **17**, 2851–2865, https://doi.org/10.1175/1520-0442(2004)017<2851:TAAIT>2.0.CO;2.

Dong, B., J. M. Gregory, and R. T. Sutton, 2009: Understanding land–sea warming contrast in response to increasing greenhouse gases. Part I: Transient adjustment. *J. Climate*, **22**, 3079–3097, https://doi.org/10.1175/2009JCLI2652.1.

Donohue, R. J., M. L. Roderick, T. R. McVicar, and G. D. Farquhar, 2013: Impact of CO_2 fertilization on maximum foliage cover across the globe's warm, arid environments. *Geophys. Res. Lett.*, **40**, 3031–3035, https://doi.org/10.1002/grl.50563.

Frierson, D. M. W., 2007: The dynamics of idealized convection schemes and their effect on the zonally averaged tropical circulation. *J. Atmos. Sci.*, **64**, 1959–1976, https://doi.org/10.1175/JAS3935.1.

Gates, W. L., 1992: AMIP: The Atmospheric Model Intercomparison Project. *Bull. Amer. Meteor. Soc.*, **73**, 1962–1970, https://doi.org/10.1175/1520-0477(1992)073<1962:ATAMIP>2.0.CO;2.

Geen, R., F. H. Lambert, and G. K. Vallis, 2018: Regime change behavior during Asian Monsoon onset. *J. Climate*, **31**, 3327–3348, https://doi.org/10.1175/JCLI-D-17-0118.1.

——, ——, and ——, 2019: Processes and timescales in onset and withdrawal of ''aquaplanet monsoons.'' *J. Atmos. Sci.*, **76**, 2357–2373, https://doi.org/10.1175/JAS-D-18-0214.1.

Gill, A. E., 1980: Some simple solutions for heat-induced tropical circulation. *Quart. J. Roy. Meteor. Soc.*, **106**, 447–462, https://doi.org/10.1002/qj.49710644905.

IPCC, 2013: Summary for policymakers. *Climate Change 2013: The Physical Science Basis*, T. F. Stocker et al., Eds., Cambridge University Press, 1–29.

Jiménez-Esteve, B., and D. I. V. Domeisen, 2019: Nonlinearity in the North Pacific atmospheric response to a linear ENSO forcing. *Geophys. Res. Lett.*, **46**, 2271–2281, https://doi.org/10.1029/2018GL081226.

Kooperman, G. J., Y. Chen, F. M. Hoffman, C. D. Koven, K. Lindsay, M. S. Pritchard, A. L. S. Swann, and J. T. Randerson, 2018: Forest response to rising CO_2 drives zonally asymmetric rainfall change over tropical land. *Nat. Climate Change*, **8**, 434–440, https://doi.org/10.1038/s41558-018-0144-7.

Laguë, M. M., and A. L. Swann, 2016: Progressive midlatitude afforestation: Impacts on clouds, global energy transport, and precipitation. *J. Climate*, **29**, 5561–5573, https://doi.org/10.1175/JCLI-D-15-0748.1.

——, G. B. Bonan, and A. L. S. Swann, 2019: Separating the impact of individual land surface properties on the terrestrial surface energy budget in both the coupled and uncoupled land–atmosphere system. *J. Climate*, **32**, 5725–5744, https://doi.org/10.1175/JCLI-D-18-0812.1.

——, M. Pietschnig, S. Ragen, T. A. Smith, and D. S. Battisti, 2021: Terrestrial evaporation and global climate: Lessons from Northland, a planet with a hemispheric continent. *J. Climate*, **34**, 2253–2276, https://doi.org/10.1175/JCLI-D-20-0452.1.

Langenbrunner, B., M. S. Pritchard, G. J. Kooperman, and J. T. Randerson, 2019: Why does Amazon precipitation decrease when tropical forests respond to increasing CO_2? *Earth's Future*, **7**, 450–468, https://doi.org/10.1029/2018EF001026.

Liu, Q., M. Collins, P. Maher, S. I. Thomson, and G. K. Vallis, 2021: SimCloud version 1.0: A simple diagnostic cloud scheme for idealized climate models. *Geosci. Model Dev.*, **14**, 2801–2826, https://doi.org/10.5194/gmd-14-2801-2021.

Mahowald, N., F. Lo, Y. Zheng, L. Harrison, C. Funk, D. Lombardozzi, and C. Goodale, 2016: Projections of leaf area index in Earth system models. *Earth Syst. Dyn.*, **7**, 211–229, https://doi.org/10.5194/esd-7-211-2016.

Manabe, S., 1969: Climate and the ocean circulation. *Mon. Wea. Rev.*, **97**, 739–774, https://doi.org/10.1175/1520-0493(1969)097<0739:CATOC>2.3.CO;2.

——, R. J. Stouffer, M. J. Spelman, and K. Bryan, 1991: Transient responses of a coupled ocean–atmosphere model to gradual changes of atmospheric CO_2. Part I: Annual mean response. *J. Climate*, **4**, 785–818, https://doi.org/10.1175/1520-0442(1991)004<0785:TROACO>2.0.CO;2.

Martinez, J. A., and F. Dominguez, 2014: Sources of atmospheric moisture for the La Plata River basin. *J. Climate*, **27**, 6737–6753, https://doi.org/10.1175/JCLI-D-14-00022.1.

Milly, P. C. D., 1994: Climate, soil water storage, and the average annual water balance. *Water Resour. Res.*, **30**, 2143–2156, https://doi.org/10.1029/94WR00586.

——, and K. A. Dunne, 2016: Potential evapotranspiration and continental drying. *Nat. Climate Change*, **6**, 946–949, https://doi.org/10.1038/nclimate3046.

Mlawer, E. J., S. J. Taubman, P. D. Brown, M. J. Iacono, and S. A. Clough, 1997: Radiative transfer for inhomogeneous atmospheres: RRTM, a validated correlated-k model for the longwave. *J. Geophys. Res.*, **102**, 16 663–16 682, https://doi.org/10.1029/97JD00237.

Monteith, J. L., 1981: Evaporation and surface temperature. *Quart. J. Roy. Meteor. Soc.*, **107**, 1–27, https://doi.org/10.1002/qj.49710745102.

Neelin, J. D., and I. M. Held, 1987: Modeling tropical convergence based on the moist static energy budget. *Mon. Wea. Rev.*, **115**, 3–12, https://doi.org/10.1175/1520-0493(1987)115<0003:MTCBOT>2.0.CO;2.

Nie, J., W. R. Boos, and Z. Kuang, 2010: Observational evaluation of a convective quasi-equilibrium view of monsoons. *J. Climate*, **23**, 4416–4428, https://doi.org/10.1175/2010JCLI3505.1.

Osborne, J. M., and F. H. Lambert, 2018: A simple tool for refining GCM water availability projections, applied to Chinese catchments. *Hydrol. Earth Syst. Sci.*, **22**, 6043–6057, https://doi.org/10.5194/hess-22-6043-2018.

Penman, H. L., 1948: Natural evaporation from open water, bare soil and grass. *Proc. Roy. Soc. London*, **193**, 120–145, https://doi.org/10.1098/rspa.1948.0037.

Pietschnig, M., 2020: Understanding changes in tropical precipitation due to climate change. Ph.D. thesis, University of Exeter, 171 pp., http://hdl.handle.net/10871/123634.

——, F. H. Lambert, M. Saint-Lu, and G. K. Vallis, 2019: The presence of Africa and limited soil moisture contribute to future drying of South America. *Geophys. Res. Lett.*, **46**, 12 445–12 453, https://doi.org/10.1029/2019GL084441.

Saint-Lu, M., R. Chadwick, F. H. Lambert, and M. Collins, 2019: Surface warming and atmospheric circulation dominate rainfall changes over tropical rainforests under global warming. *Geophys. Res. Lett.*, **46**, 13 410–13 419, https://doi.org/10.1029/2019GL085295.

Scheff, J., and D. M. W. Frierson, 2014: Scaling potential evapotranspiration with greenhouse warming. *J. Climate*, **27**, 1539–1558, https://doi.org/10.1175/JCLI-D-13-00233.1.

Seager, R., N. Naik, and G. A. Vecchi, 2010: Thermodynamic and dynamic mechanisms for large-scale changes in the hydrological cycle in response to global warming. *J. Climate*, **23**, 4651–4668, https://doi.org/10.1175/2010JCLI3655.1.

Sellers, P. J., and Coauthors, 1996: Comparison of radiative and physiological effects of doubled atmospheric CO_2 on climate. *Science*, **271**, 1402–1406, https://doi.org/10.1126/science.271.5254.1402.

Shi, X., and D. R. Durran, 2014: Estimating the response of extreme precipitation over midlatitude mountains to global warming. *J. Climate*, **28**, 4246–4262, https://doi.org/10.1175/JCLI-D-14-00750.1.

Shukla, J., and Y. Mintz, 1982: Influence of land-surface evapotranspiration on the Earth's climate. *Science*, **215**, 1498–1501, https://doi.org/10.1126/science.215.4539.1498.

Skinner, C. B., C. J. Poulsen, R. Chadwick, N. S. Diffenbaugh, and R. P. Fiorella, 2017: The role of plant CO_2 physiological forcing in shaping future daily-scale precipitation. *J. Climate*, **30**, 2319–2340, https://doi.org/10.1175/JCLI-D-16-0603.1.

——, ——, and J. S. Mankin, 2018: Amplification of heat extremes by plant CO_2 physiological forcing. *Nat. Commun.*, **9**, 1094, https://doi.org/10.1038/s41467-018-03472-w.

Spracklen, D. V., S. R. Arnold, and C. M. Taylor, 2012: Observations of increased tropical rainfall preceded by air

passage over forests. *Nature*, **489**, 282–285, https://doi.org/10.1038/nature11390.

Swann, A. L. S., 2018: Plants and drought in a changing climate. *Curr. Climate Change Rep.*, **4**, 192–201, https://doi.org/10.1007/s40641-018-0097-y.

——, F. M. Hoffman, C. D. Koven, and J. T. Randerson, 2016: Plant responses to increasing CO_2 reduce estimates of climate impacts on drought severity. *Proc. Natl. Acad. Sci. USA*, **113**, 10 019–10 024, https://doi.org/10.1073/pnas.1604581113.

Taylor, K. E., R. J. Stouffer, and G. A. Meehl, 2012: An overview of CMIP5 and the experiment design. *Bull. Amer. Meteor. Soc.*, **93**, 485–498, https://doi.org/10.1175/BAMS-D-11-00094.1.

Thomson, S. I., and G. K. Vallis, 2019: Hierarchical modeling of solar system planets with Isca. *Atmosphere*, **10**, 803, https://doi.org/10.3390/atmos10120803.

Vallis, G. K., and Coauthors, 2018: Isca, v1.0: A framework for the global modelling of the atmospheres of Earth and other planets at varying levels of complexity. *Geosci. Model Dev.*, **11**, 843–859, https://doi.org/10.5194/gmd-11-843-2018.

van der Ent, R. J., H. H. G. Savenije, B. Schaefli, and S. C. Steele-Dunne, 2010: Origin and fate of atmospheric moisture over continents. *Water Resour. Res.*, **46**, https://doi.org/10.1029/2010WR009127.

Voigt, A., and Coauthors, 2016: The tropical rain belts with an annual cycle and a continent model intercomparison project: TRACMIP. *J. Adv. Model. Earth Syst.*, **8**, 1868–1891, https://doi.org/10.1002/2016MS000748.

von Randow, C., and Coauthors, 2004: Comparative measurements and seasonal variations in energy and carbon exchange over forest and pasture in South West Amazonia. *Theor. Appl. Climatol.*, **78**, 5–26, https://doi.org/10.1007/s00704-004-0041-z.

Wills, R. C., and T. Schneider, 2015: Stationary eddies and the zonal asymmetry of net precipitation and ocean freshwater forcing. *J. Climate*, **28**, 5115–5133, https://doi.org/10.1175/JCLI-D-14-00573.1.

Wright, J. S., R. Fu, J. R. Worden, S. Chakraborty, N. E. Clinton, C. Risi, Y. Sun, and L. Yin, 2017: Rainforest-initiated wet season onset over the southern amazon. *Proc. Natl. Acad. Sci. USA*, **114**, 8481–8486, https://doi.org/10.1073/pnas.1621516114.

Zarakas, C. M., A. L. S. Swann, M. M. Laguë, K. C. Armour, and J. T. Randerson, 2020: Plant physiology increases the magnitude and spread of the transient climate response to CO2 in CMIP6 Earth system models. *J. Climate*, **33**, 8561–8578, https://doi.org/10.1175/JCLI-D-20-0078.1.

Zelinka, M. D., T. A. Myers, D. T. McCoy, S. Po-Chedley, P. M. Caldwell, P. Ceppi, S. A. Klein, and K. E. Taylor, 2020: Causes of higher climate sensitivity in CMIP6 models. *Geophys. Res. Lett.*, **47**, e2019GL085782, https://doi.org/10.1029/2019GL085782.

Zhang, L., K. Hickel, W. R. Dawes, F. H. S. Chiew, A. W. Western, and P. R. Briggs, 2004: A rational function approach for estimating mean annual evapotranspiration. *Water Resour. Res.*, **40**, W02502, https://doi.org/10.1029/2003WR002710.